Thermal Management of Quantum Cascade Lasers in an Individually Addressable Monolithic Array Architecture

Leo Missaggia, Christine Wang, Michael Connors, Brian Saar, Antonio Sanchez-Rubio
Kevin Creedon, George Turner, William Herzog

Lincoln Laboratory, Massachusetts Institute of Technology
244 Wood Street, Lexington, MA 02420
Distribution A: Public Release

Abstract

There are a number of military and commercial applications for high-power laser systems in the mid-to-long-infrared wavelength range. By virtue of their demonstrated watt-level performance and wavelength diversity, quantum cascade laser (QCL) and amplifier devices are an excellent choice of emitter for those applications. To realize the power levels of interest, beam combining of arrays of these emitters is required and as a result, array technology must be developed. With this in mind, packaging and thermal management strategies were developed to facilitate the demonstration of a monolithic QCL array operating under CW conditions. Thermal models were constructed and simulations performed to determine the effect of parameters such as array-element ridge width and pitch on gain region temperature rise. The results of the simulations were considered in determining an appropriate QCL array configuration. State-of-the-art micro-impingement cooling along with an electrical distribution scheme comprised of AlN multi-layer technology were integrated into the design. The design of the module allows for individual electrical addressability of the array elements, a method of phase control demonstrated previously for coherent beam combining of diode arrays, along with access to both front and rear facets. Hence, both laser and single-pass amplifier arrays can be accommodated. A module was realized containing a 5 mm cavity length monolithic QCL array comprised of 7 elements on 450 μm pitch. An output power of 3.16 W was demonstrated under CW conditions at an emission wavelength of 9 μm.

OCIS codes: Semiconductor lasers, quantum cascade (140.5965), Laser arrays (140.3290)

1. Introduction

High power laser systems operating in the mid-infrared spectral band are of great interest for a number of military applications. Examples of these applications include remote sensing and infrared countermeasures. Quantum cascade lasers (QCLs) are an attractive light source for these applications in that they are watt-class semiconductor emitters which have been demonstrated, operating under room temperature CW conditions, over a spectral band from 3 μm to beyond 14 μm. In order to realize systems capable of producing the power levels required to satisfy some applications of interest, beam combining of arrays of these devices would be required. In this work packaging and thermal management strategies were developed to facilitate the CW operation of a long-wave infrared (LWIR) monolithic QCL array as a prerequisite for coherent beam combining (CBC) demonstrations.

CBC of semiconductor emitter arrays has been an ongoing effort at MIT Lincoln Laboratory for well over a decade. Successful CBC of arrays of semiconductor diode emitters operating at ~ 1 μm have been demonstrated, where record beam combined powers were achieved [1]. Most recently CBC of a 2-element mid-wave infrared (MWIR) quantum cascade single-pass amplifier (QCA) array was also demonstrated [2]. There are a number of considerations with regards to the design of the packaging architecture required to facilitate the CBC of emitter arrays containing large numbers of elements, depending upon whether the utilization is for single-pass amplifiers or lasers. These considerations include aggressive thermal management, individual electrical addressability of array elements, and in the case of single-pass amplifier arrays, access to both front and rear array facets. There are several characteristics of QCL device performance which make QCL array architectures thermally challenging. Among these are;

  1.   Relatively low electrical-to-optical power conversion efficiency (PCE).

2. High series resistance requiring relatively large voltages to achieve high-power operation.
3. Anisotropic and extremely poor thermal conductivity of the gain region which can be as low as 2.0 to 4.0 W/m-°C depending upon the direction of heat flow.

The low PCE combined with operation of these devices at watt-level optical outputs results in relatively large power dissipation per array element.

Figure 1 shows a micrograph image of the cross section of a realized LWIR QCL device along with its electro-optical performance. The design of the device was based on a single phonon-continuum depopulation structure [3] and grown via OMVPE [4]. The device had a 12 μm wide gain region and a 5 mm cavity length. A high-reflectivity coating (R > 95%) was deposited on the rear facet. The QCL operating CW shows a maximum output power of ~ 1.0 W with a PCE of ~ 6.25 %. Therefore, the waste heat generated by this device within the gain region was ~ 16.0 W. As a case in point, for a 1 cm wide array comprised of similar QCL elements on a 200 μm pitch, the total waste heat generated would be ~ 800 W resulting in a power dissipation per unit area of ~ 1600 W/cm^2. Heat fluxes of this magnitude require high performance cooling technology along with an understanding of the thermal impact on the array elements for chosen array geometries, i.e., the operating temperature of the gain region and how it is affected by parameters such as the array element pitch and ridge width. Insight into these relationships was achieved through thermal simulations which were important in guiding the design of array geometries to obtain acceptable array performance.
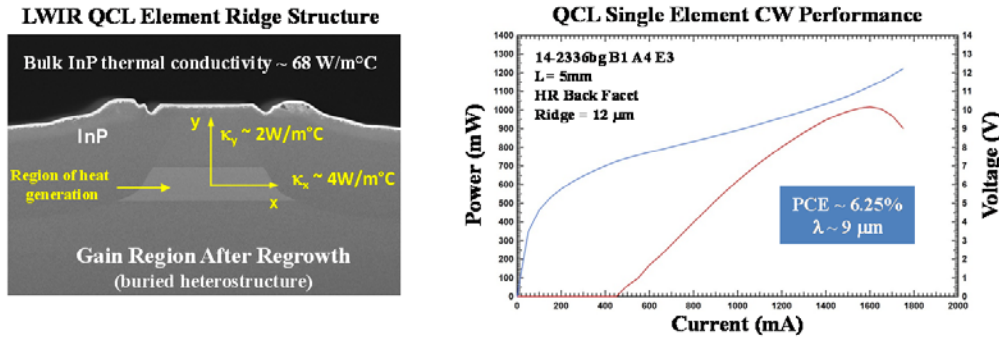

Figure 1. (a) Micrograph of QCL ridge structure. (b) CW electro-optical performance.

2. Thermal Simulations

To investigate the relationship between the temperature rise of the gain region of a QCL array element and array geometry, a finite-element model (FEM) of a QCL device was constructed and is shown in figure 2. Invoking symmetry, this periodic structure represents a single element of an array comprised of an infinite number of elements. Hence, the array-element pitch can be varied by adjusting the overall width of the model. All pertinent layers comprising the QCL structure such as the gain region, InP cladding, InP regrowth regions and substrate along with an electrical bus contact layer above and a metalized AlN carrier below were included in the model. The temperature dependence of the thermal conductivities of the various layers comprising the QCL structure were included, along with the anisotropic thermal conductivity of the gain region [5]. A volumetric heat load was applied to the gain region of the model representative of the expected optical output power, PCE, gain region width (effective ridge width) and cavity length. The lower boundary condition represented that of the thermal performance of a state-of-the-art micro-impingement cooler, technology employed as part of the overall module design. All other boundaries were assumed adiabatic. Simulations were run for the following conditions;

1. 1.0 W optical output power per element.
2. PCE of 5% and 10%, (lower and upper boundaries of expected element performance)

3. Effective ridge widths of 10, 12 and 14 μm.
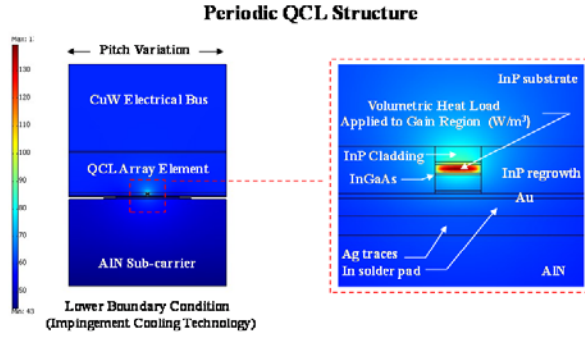4. Variation in pitch of array elements from 75 to 600 μm.

Periodic QCL Structure

Figure 2. FEM of periodic QCL array structure.

The results of the simulations for an array having a cavity length of 5 mm are shown in figure 3. The curves illustrate the relationship among the temperature rise within the gain region of an element, the array element pitch, and ridge width. The simulations predict thermal crowding (cross talk) between array elements begins to dominate, in the form of significantly increasing gain region temperature, as the pitch of the array drops below 300 μm.
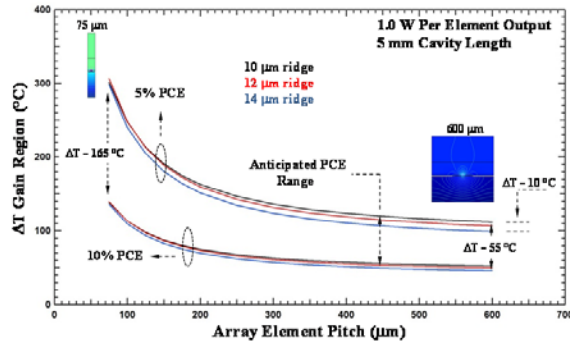

Figure 3. Predicted temperature rise of a QCL array element gain region as a function of array element pitch.

The difference in gain-region temperature rise between array elements operating at 10% and 5% PCE is ~ 55 °C at the widest array pitch (600 μm) and increases to ~ 165 °C at the narrowest pitch (75 μm). As the pitch of the array elements is decreased, the ability for 2-D heat flow away the gain region is reduced and the overall power dissipation generated by the array has a greater effect on the temperature of the gain region. The ridge widths chosen for the simulations represent widths in which watt-level powers were produced experimentally while maintaining single spatial mode emission, important for demonstrating high power with high combining efficiency. For the ridge width range of 10 to 14 μm, the comparison ΔT for a given array pitch is ~ 10 °C, with the wider ridges predicted cooler. Although the heat transfer out of the gain region would be less efficient for devices with wider ridges (poor thermal conductivity within that region), the power dissipation per unit volume is smaller for the same PCE and emission power. As a result elements with narrower ridges show a slightly higher gain region temperature rise. Based on the results of these simulations, and in an attempt to minimize the thermal cross talk between array elements while maintaining an acceptable optical output

power per-cm bar width, the pitch, ridge width, and cavity length of the array were chosen as 450 μm, 12 μm, and 5 mm respectively for the initial monolithic QCL array demonstration.

3. QCL Array Module Architecture

As an initial demonstration of a monolithic QCL array, the module was designed to accommodate an array comprised of up to 9 elements. Based on the performance of the single-element QCL described earlier and the array geometry chosen the predicted power dissipation of a 9 element array is ~ 700 W/cm^2. A commercially available state-of-the-art micro-impingement cooler was employed to handle the heat flux. These high performance coolers have thermal resistances on the order of 0.03 °C-cm^2/W resulting in a modest temperature rise at the cooling surface of ~ 21°C at a uniform heat flux of 700 W/cm^2. Figure 4a shows an image of the impingement cooler which has been customized to accommodate the facet access requirement for a single-pass amplifier array. Front and rear recesses have been machined into the cooling surface to accommodate a 5 mm cavity length.
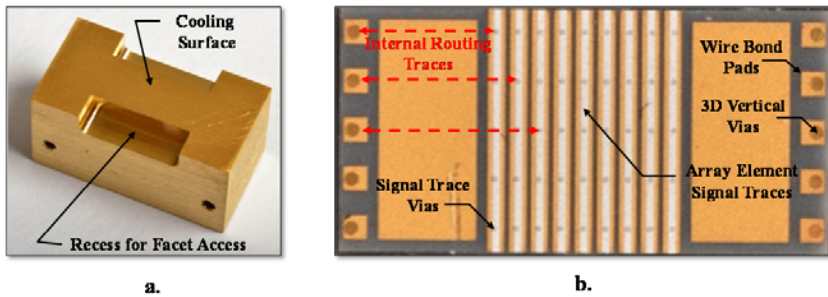

Figure 4. (a) High performance micro-impingement cooler. (b) AlN multilayer carrier.

CBC phase control of the array elements was achieved via current adjustment [1,2]. Therefore, individual electrical addressability of the array elements is required, with the added complexity of maintaining front and rear facet access. This was achieved by designing a current distribution scheme whose key component was an AlN multilayer carrier. The carrier design uses 3-D internal routing of electrical traces, which connect each individual element of the array to a designated bond pad at the perimeter of the carrier by way of vertical vias. The internal structure of the carrier was fabricated commercially followed by post processing of the carrier, performed at MIT-LL, where a top-surface thin-film metallization scheme was deposited and patterned. The carrier was then diced such that the dimension relative to the cavity length of the array was ~ 10 to 15 μm less than that of the array, allowing for a slight overhang of the array with respect to the carrier. A fully processed carrier is shown in figure 4b. A series of alignment and reflow soldering procedures [6] were used to assemble the array to the carrier followed by the array/carrier assembly to the cooler. A schematic of an exploded view of the components comprising the module is shown in figure 5 along with a fully assembled module. Wire-bond connections were made from the perimeter bond pads of the AlN carrier to printed circuit boards with connectors attached allowing for electrical bias of the individual array elements. A manifold was integrated into the design to direct coolant to and from the impingement cooler. The module was designed to accommodate both laser and single-pass amplifier arrays. However, the initial module demonstration was with a laser array to avoid the added complexity of seeding amplifiers. Although the module could accommodate an array of up to 9 elements the initial packaging exercise was of a 7-element monolithic QCL array.
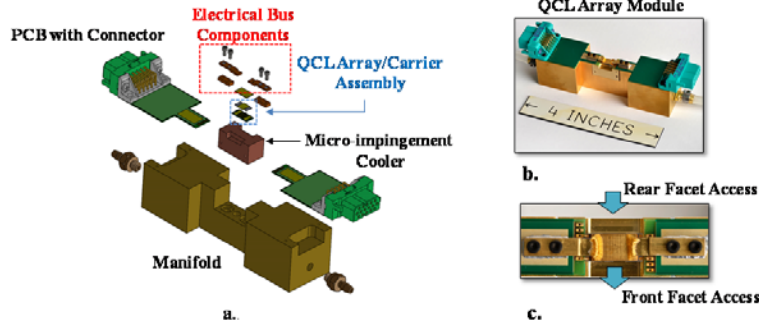
Figure 5. (a) Exploded view of components comprising module. (b) Realized module. (c) Top view illustrating facet access.

4. Monolithic QCL Array Performance

Each element's performance was initially characterized prior to the simultaneous operation of the entire array. The individual array element CW performance can be seen in the curves shown in figure 6a. Note that there were no optical coatings deposited on the facets of the array so the power is shown per facet. The variation in maximum output power ranged from ~ 0.73 W to 0.86 W with a maximum efficiency of ~ 5.5 %. A Fourier Transform Infrared (FTIR) spectrometer was used to measure the emissions wavelength from the individual emitters. Wavelength measurements were taken at current levels linked with peak powers (~ 1.6 A) and indicate all emitters operating near 9 μm as shown in figure 6b. Once the performances of the individual elements of the array were characterized, the elements were biased simultaneously to demonstrate true monolithic array operation. The performance of the array with all 7 elements operating simultaneously is shown in figure 7. The total output power was ~ 3.16 W, illustrated by the red curve. Although thermal simulations were performed as guidance in determining an array configuration to help minimize thermal cross talk between array elements, the intrinsic thermal cross talk present during array operation affected the performance of the elements as illustrated by the comparison between the blue and red curves. The blue curve represents the summation of all the individual elements CW performance curves shown in figure 6a, illustrating the array performance if thermal cross-talk between elements was nonexistent. Both a decrease in I_{th} along with increased output power and efficiency would be expected. The output power predicted from the summation of the individual element performance curves was ~ 5.46 W, corresponding to an increase in output power of ~ 40%. Clearly reducing the overall thermal resistance of the array module or increasing the PCE of the array elements would further enhance array performance.
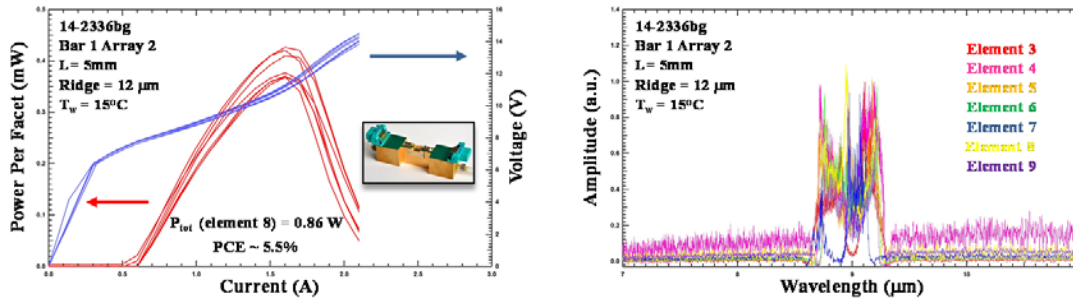

Figure 6. (a) Individual array element CW performance. (b) Array element emission wavelength.
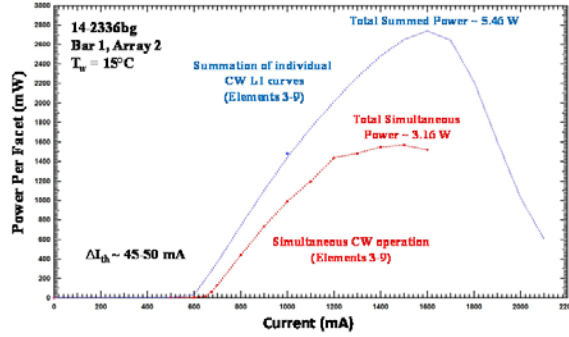
Figure 7. Simultaneous array element CW operation.

5. Validation of Thermal Modeling

Since thermal simulations were used as guidance in determining the array configuration and the overall design of the module, validation of this modeling is important. The experimentally--demonstrated performance of the 7-element QCL array module was used for this validation. To perform this validation the QCL material was characterized for its performance dependence with operating temperature. An unpackaged QCL element was operated under pulsed conditions using a 200 ns pulse width at 1 KHz frequency. The corresponding duty cycle, 0.02%, ensured that no self-heating within the gain region occurred during operation. Performance curves were generated over a temperature range from ~ 14 °C to 100 °C as shown in figure 8a. As expected, there is a significant increase in the threshold current (I_{th}) of the device as its temperature is increased. In figure 8b, the operating temperature of the device was plotted versus the measured threshold current. The relationship between the gain region temperature and corresponding change in I_{th} was found to be ~ 210 °C per amp of threshold current shift.
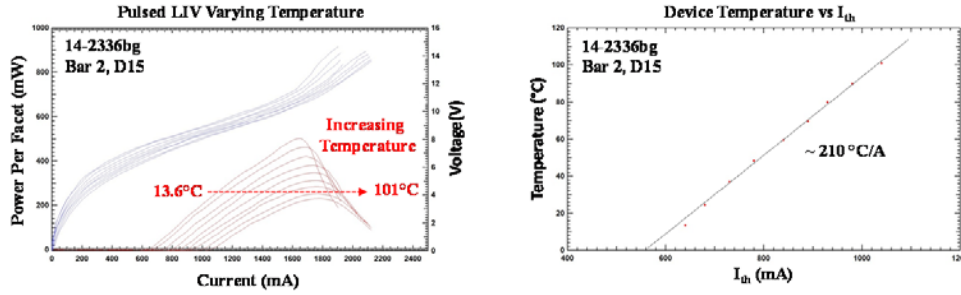

Figure 8. (a) Pulsed electro-optical performance with temperature. (b) Threshold current dependence on temperature.

Since there is individual electrical addressability of the array elements, a known thermal load can be imposed upon a given array element via biasing of adjacent elements and the change in I_{th} of an element operating under CW conditions with and without thermal loading could be observed. The emitters of the 7-element array were designated as elements 3 through 9 within the realized module, with element 6 being the central element. If biased just below threshold, elements adjacent to element 6 could be utilized as heat loads with no optical output contribution to that of the performance of element 6. Under these two conditions the CW electro-optical performance of element 6 is shown in the curves of figure 9. The lowest threshold, highest output power curve (red) is that of element 6 operating with no heat load from any of

the adjacent array elements. The highest threshold, lowest output power curve (blue) represents the performance of element 6 with all other array elements biased just below lasing threshold. The observed increase in I_{th} is ~ 50 mA.
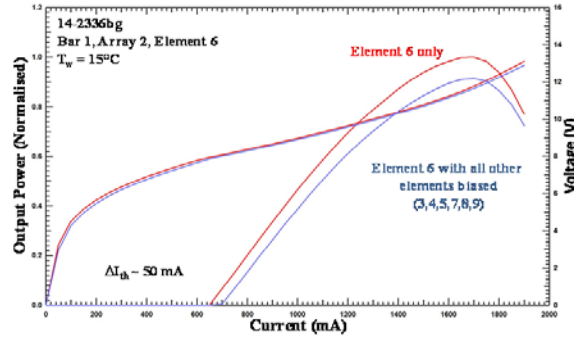

Figure 9. CW performance of element 6 with and without thermal load from adjacent array elements.

In order to proceed with the validation, an appropriate FEM model representative of the design of the existing 9 element module architecture was constructed and can be seen in figure 10a. The model is comprised of the QCL array, a CuW electrical bus above and an AlN carrier below. The model includes all pertinent layers within the QCL structure along with the appropriate boundary conditions. There are 9 representative elements and corresponding gain regions where parasitic heat loads can be applied. The ability to independently "turn on" the power dissipation within the representative gain region of an array element allows for the prediction of the temperature rise of a given array element, for any combination of operating elements. The shift in I_{th} due to a specific thermal loading, and illustrated experimentally, can be reproduced theoretically in the form of a temperature rise within the gain region. Simulations were performed for the two cases experimentally demonstrated where the central element was operated independently, followed by operation with parasitic heat loads applied via bias just below I_{th} of the other 6 elements. Using the known current and voltage values at lasing threshold for the array elements, the corresponding power dissipation was calculated and applied as a volumetric heat load within the appropriate gain regions of the model. The typical power dissipation for a given array element at I_{th} was ~ 4.5 W.
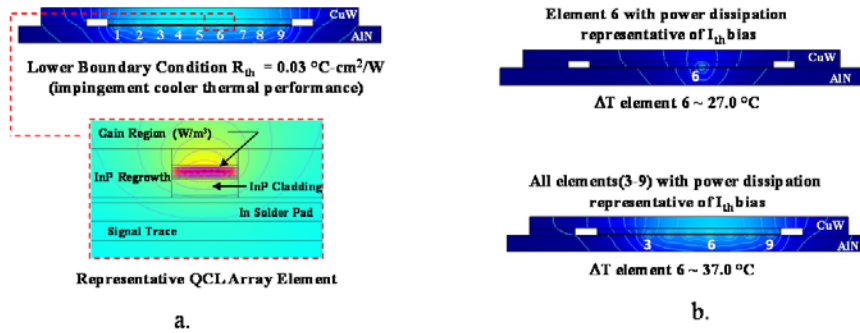

Figure 10. (a) FE model of 9 element array module. (b) Simulations for element 6 with and without adjacent thermal loads.

The results of the simulations are shown in figure 10b. For the case where a heat load was applied to the central element (element 6), representative of the power dissipation at I_{th}, the temperature rise within the gain region was predicted to be ~ 27 °C. For the case where heat loads were applied to all of the array elements, again representative of their power dissipation at I_{th}, the temperature rise of the central element was predicted to be ~ 37 °C. The change in temperature of

the representative gain region of element 6 for the two cases is ~ 10 °C. Utilizing the experimentally determined relationship between gain region temperature rise and threshold current shift (210 °C/A) the expected increase in I_{th} under the modeling conditions described above would be ~ 47 mA. This prediction is within 6% of the experimentally measured threshold shift of ~ 50 mA, confirming the fidelity of the thermal modeling approach and verifying confidence in moving forward with predicting the thermal performance of QCL array architectures.

6. Summary

In summary, packaging and thermal management strategies were developed to facilitate the demonstration of a monolithic QCL array operating under CW conditions. The design of the module allowed for individual electrical addressability of the array elements along with access to the front and rear array facets, thus accommodating future CBC demonstrations of either laser or single-pass amplifier arrays. As part of the initial design process thermal models were constructed and simulations were performed to assist in the design of the array configuration. A module was realized comprised of a 5 mm cavity length QCL array containing 7 elements on 450 μm pitch. Electro-optical characterization of both the individual element performance and simultaneous array element operation was performed. The total power measured for the array elements operating simultaneously was 3.16 W at an emission wavelength of ~ 9 μm. A validation of the thermal modeling approach was performed utilizing array performance data obtained experimentally. The theoretical thermal predictions were found to be in good agreement with the experimental data thus confirming the fidelity of the thermal modeling.

References

1.   S. M. Redmond, K. J. Creedon, J. E. Kansky, S. J. Augst, L. J. Missaggia, M. K. Connors, R. K. Huang, B. Chann, T. Y. Fan, G. W. Turner, and A. Sanchez-Rubio, "Active coherent beam combining of diode lasers," *Opt. Lett. 36, 999-1001 (2011).*

2.   B. G. Saar, K. Creedon, L. Missaggia, C. A. Wang, M. K. Connors, J. Donnelly, G. W. Turner, A. Sanchez-Rubio, and W. Herzog, "Coherent Beam-Combining of Quantum Cascade Amplifier Arrays," in *CLEO: 2015, OSA Technical Digest (online) (Optical Society of America, 2015), paper STu4G.3.*

3.   K. Fujita, S. Furuta, A. Sugiyama, T. Ochiai, T. Edamura, N. Akikusa, M. Yamanishi, and H. Kan, "High-Performance l ~ 8.6 mm Quantum Cascade Lasers With Single Phonon-Continuum Depopulation Structures," *Quantum Electronics, IEEE Journal of*, vol. 46, pp. 683-688, 2010.

4.   C. A. Wang, A. K. Goyal, S. Menzel, D. R. Calawa, M. Spencer, M. K. Connors, D. McNulty, A. Sanchez, G. W. Turner, and F. Capasso, "High power (>5 W) l~9.6 mm tapered quantum cascade lasers grown by OMVPE," *Journal of Crystal Growth, vol. 370, pp. 212-216, 2013.*

5.   Antonia Lops, Vincenzo Spagnolo, [a] and Gaetano Scarmarcio, "Thermal Modeling of GaInAs/AlInAs quantum cascade lasers", *Journal of Applied Physics 100, 043109 (2006).*

6.   L. J. Missaggia, R. K. Huang, B. Chann, R. Swint, J. P. Donnelly, A. Sanchez-Rubio, G. W. Turner, "Packaging and Thermal Management of High-Power, Slab-Coupled Optical Waveguide Laser Arrays for Beam Combining," in *Electronic Components and Technology Conference, 2008. ECTC 2008. 58th , vol., no., pp.998-1004, 27-30 May 2008*